Karlsson *et al. Artery Research* (2022) 28:113-127
https://doi.org/10.1007/s44200-022-00022-0

Artery Research

RESEARCH ARTICLE

Open Access

Abdominal Aortic Wall Cross-coupled Stiffness Could Potentially Contribute to Aortic Length Remodeling

Jerker Karlsson[1,2*], Jonas Stålhand[3], Carl-Johan Carlhäll[1,2,5], Toste Länne[2,4] and Jan Engvall[1,2,5]

Abstract

Background: Wall stiffness of the abdominal aorta is an important factor in the cardiovascular risk assessment. We investigated abdominal aortic wall stiffness divided in direct and cross-coupled stiffness components with respect to sex and age.

Methods: Thirty healthy adult males ($n = 15$) and females were recruited and divided into three age groups: young, middle aged and elderly. Pulsatile diameter changes were determined noninvasively by an echo-tracking system, and intra-aortic pressure was measured simultaneously. A mechanical model was used to compute stress and stiffness in circumferential and longitudinal directions.

Results: Circumferential stretch had a higher impact on longitudinal wall stress than longitudinal stretch had on circumferential wall stress. Furthermore, there were an age-related and sex-independent increase in circumferential and longitudinal direct and cross-coupled stiffnesses and a decrease in circumferential and longitudinal stretch of the abdominal aortic wall. For the young group, females had a stiffer wall compared to males, while the male aortic wall grew stiffer with age at a higher rate, reaching a similar level to that of the females in the elderly group.

Conclusion: Temporal changes in aortic stiffness suggest an age-related change in wall constituents that is expressed in terms of circumferential remodeling impacting longitudinal stress. These mechanisms may be active in the development of aortic tortuosity. We observed an age-dependent increase in circumferential and longitudinal stiffnesses as well as decrease in stretch. A possible mechanism related to the observed changes could act via chemical alterations of wall constituents and changes in the physical distribution of fibers. Furthermore, modeling of force distribution in the wall of the human abdominal aorta may contribute to a better understanding of elastin–collagen interactions during remodeling of the aortic wall.

Keywords: Abdominal aorta, Cardiovascular disease, Wall stress, Cross-coupled stiffness, Sex, Age, Remodeling, Tortuosity

1 Introduction

The mechanical properties of the aorta are important to its physiological function. The concept of hemodynamic homeostasis enables large arteries such as the aorta to transform central pulsatile pressure and flow into continuous pressure and flow in the peripheral arterioles. In this transformation, central artery stiffness has been identified as a major independent risk factor for cardiovascular disease morbidity and overall mortality [1].

Toste Länne: Deceased.

*Correspondence: jerker.karlsson@liu.se

[1] Department of Clinical Physiology in Linköping, Linköping University, 581 83 Linköping, Sweden
Full list of author information is available at the end of the article

Arterial stiffness is attributed to, e.g., extracellular matrix (ECM) components, mainly elastin and collagen, vascular smooth muscle cell (VSMC) tone, VSMC stiffness and cell–ECM interactions [2]. The cell–ECM interaction affects and regulates arterial mechanical function and structural integrity [3]. Shear as well as circumferential and longitudinal stress is key mechanical determinants of arterial wall remodeling. Aortic mechanical properties are considered to evolve from an interdependency of circumferential–longitudinal coupling of stress and stretch where stiffness may play a part [4, 5].

Stress, stiffness and stretch can be measured in vitro, but especially stress and stiffness are difficult to measure in vivo. A mechanical model, usually computerized, may be used to simulate stress, stiffness and stretch in vivo. Various mechanical models describing cardiovascular growth and remodeling have been proposed [5, 6]. We have developed a model using in vivo data with nonlinear deformation and material behavior observed for arteries to compute stress and stiffness [7, 8]. The model has been validated [9] and produced findings relevant to age- and sex-dependent changes in vessel wall constituents [10].

In biological tissue, the stress–strain curve is nonlinear, implicating nonlinear stiffness. Our mechanical model enables computation of wall stress as well as direct and cross-coupled stiffnesses from the nonlinear stress–strain curve. A commonly used variable such as Young's incremental elastic modulus calculated from stress–strain curves assumes a linear material property and is a measure of direct stiffness. In a clinical environment, aortic pulse wave velocity (PWV) is regarded as a reference parameter for central aortic stiffness [1] and mainly reflects circumferential direct stiffness. Nonlinear behavior as well as cross-coupled stiffness is much less investigated. Furthermore, cross-coupled stiffness links stretch in one direction to stress in another direction and might reveal information related to directional interdependency of stress and stretch. Therefore, the aim of this study is to investigate direct and cross-coupled stiffness and its possible implications on aortic remodeling.

2 Materials and Methods

2.1 Study Subjects

Thirty healthy, non-smoking male ($n=15$) and female volunteers without any medications were included in the study and divided in three age-groups: young (23–30 years, $n=10$), middle aged (41–54 years, $n=10$) and elderly (67–72 years, $n=10$). Exclusion criteria were a history of cardiopulmonary disease, diabetes or regular medication and an ankle brachial index < 1 suggestive of vascular obstruction. Oestrogen replacement therapy was not prescribed to anyone of the women. The acquisition of pressure and diameter is summarized below and has been described elsewhere [10].

3 Non-invasive Monitoring of Diameter Changes

Non-invasive monitoring of pulsatile diameter change in the distal abdominal aorta (AA) was carried out 3–4 cm proximal to the aortic bifurcation [10]. An electronic echo-tracking instrument (Diamove, Teltec AB, Lund, Sweden) was interfaced with a real-time ultrasound scanner (EUB-240, Hitachi, Tokyo, Japan) and fitted with a 3.5 Mhz linear array transducer. The instrument had dual echo-tracking loops; thus, two separate echoes from opposite vessel walls could be tracked simultaneously. The repetition frequency was 870 Hz, temporal resolution was 1.2 ms, and the smallest detectable displacement was 7.8 µm. For static (end diastolic and systolic) aortic diameter and for pulsatile diameter change, the coefficient of variation was 5% and 16%, respectively.

3.1 Invasive Blood Pressure Measurements

Abdominal aortic (AA) blood pressure was measured invasively at the midpoint between the renal arteries and the aortic bifurcation with a 3-F (SPC 330A) or 4-F (SPC 340) micromanometer tip catheter (Millar Instruments, Houston, TX) or with a fluid-filled catheter system (pressure monitoring kit DTX + with R.O.S.E, Viggo Spectramed, Oxnard, CA) depending on the availability. The frequency response of the Millar catheter (flat range to 10 kHz) was higher than in the fluid-filled system (flat range 35 Hz [3 dB]). However, curves from one cardiac cycle from each system were superimposed on each other using a Blood Systems Calibrator (Bio Tech Model 601 A, Old Mill Street, Burlington, VT) showing similar systolic blood pressures and pulsatile amplitude when compared.

The data acquisition system allowed for simultaneous monitoring of blood pressure and vessel diameter with a maximum registration duration of 11 s. The system contained a personal computer type 386 (Express, Tokyo, Japan) and a 12-bit analog-to-digital converter (Analogue Devices, Norwood, MA) allowing a sampling frequency of 290 Hz each for both signals. Example of acquired data is found in Fig. 1.

3.2 The Identification of Model Parameters and the Mechanical Model

The identification of model parameters and the mechanical model used have been described in previous publications [8, 10]. Also see Appendix for further information.

The parameter identification method for mechanical parameters (PIMMP) consists of two parts, a signal processing routine and a parameter identification routine

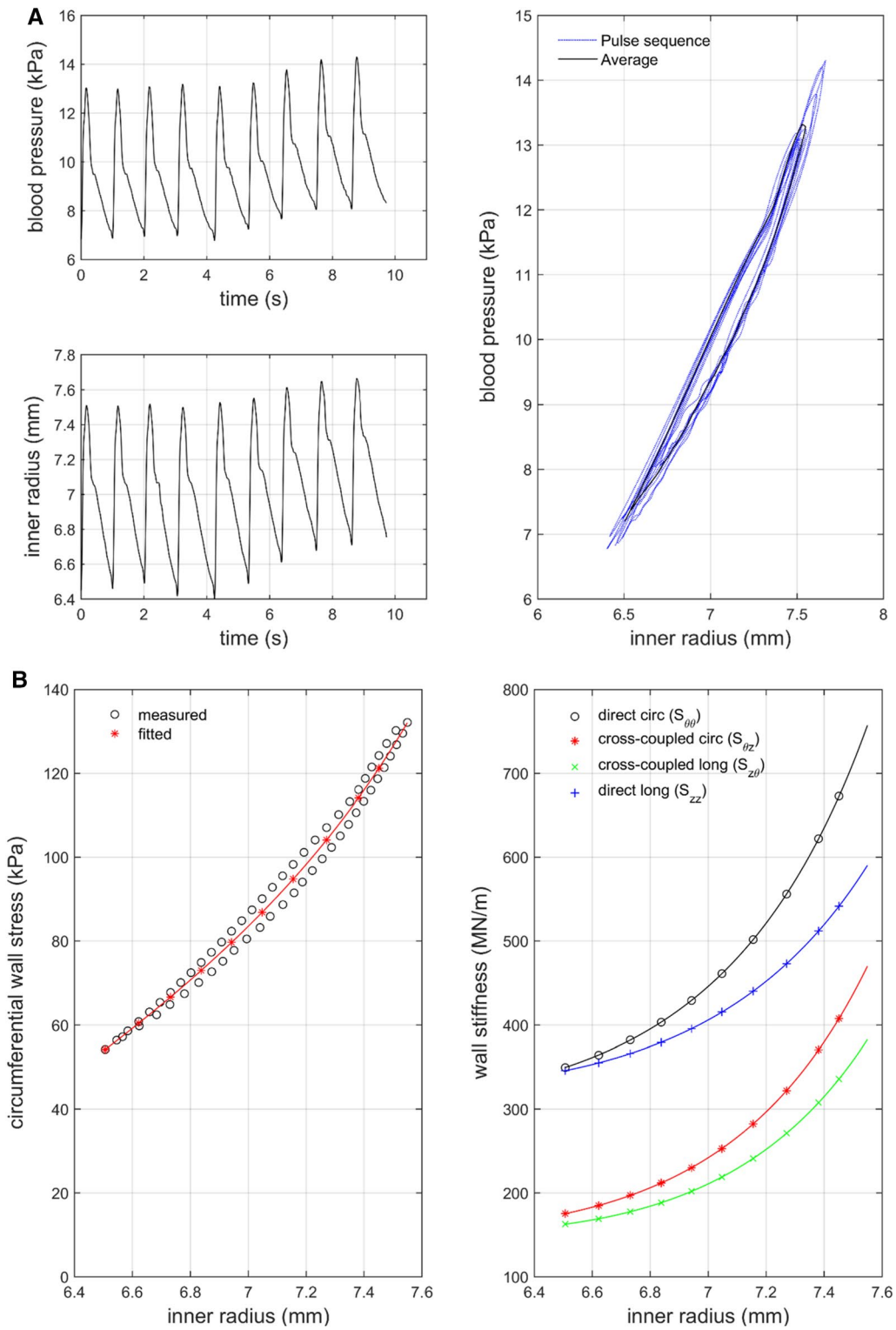

Fig. 1 Example of acquired data. **A** and **B** illustrate measured data from the abdominal aorta and identification results from PIMMP. **A** Measured blood pressure (upper left panel) and inner radius (lower left panel) for a young male. Right panel shows the pressure-radius response and the used post-processed average signal (black). **B** Left panel shows wall stress vs. inner radius in the circumferential direction for a young male. Measured data with resulting fitted curve from PIMMP representing total stress is illustrated. Right panel shows circumferential and longitudinal direct as well as cross-coupled wall stiffness vs. inner radius for a young male

including a nonlinear mechanical model. In the first part, measured blood pressure and diameter were processed in MATLAB. The data consisting of approximately 8–10 cycles (heartbeats) were lowpass filtered with a fourth-order Butterworth filter with a cutoff frequency of 15 Hz for noise reduction and automatically adjusted for time delays from the measurement setup. Furthermore, pressure and radius were averaged over cycles [8]. In part two, the model parameters were identified through a nonlinear curve fitting of the model response to the measured pressure–radius loop, according to the following iterative algorithm (Fig. 2A):

1. The stresses in the arterial wall were computed by the Laplace's law (Eq. 8 in Appendix) using the pressure-radius loop together with an estimation of the cross-sectional area (A) of the aortic wall from Åstrand et al. [11].
2. A second set of stresses was computed using nonlinear continuum mechanics (Eqs. 11 and 12) [12]. These model stresses are dependent on six model parameters (explained below) describing the material characteristics and the in situ pre-stress of the aortic wall [13–15].
3. By comparing the first set of stresses from 1 to the stresses from 2, an estimate of an error (difference) was obtained (Eq. 9) [8]. If the difference between errors from two consecutive iterations was smaller than a pre-set tolerance (typically 10^{-5}), the iteration was terminated, and the parameters were considered identified. If the error exceeded the tolerance, the parameters values were updated using standard identification techniques and steps 2 and 3 were repeated.

Six model parameters were identified, describing the characteristic (material parameters: c, k_1, k_2, β) and geometrical (geometrical parameters: R_0, and λ_z) properties of the aortic wall [10]. The parameters are:

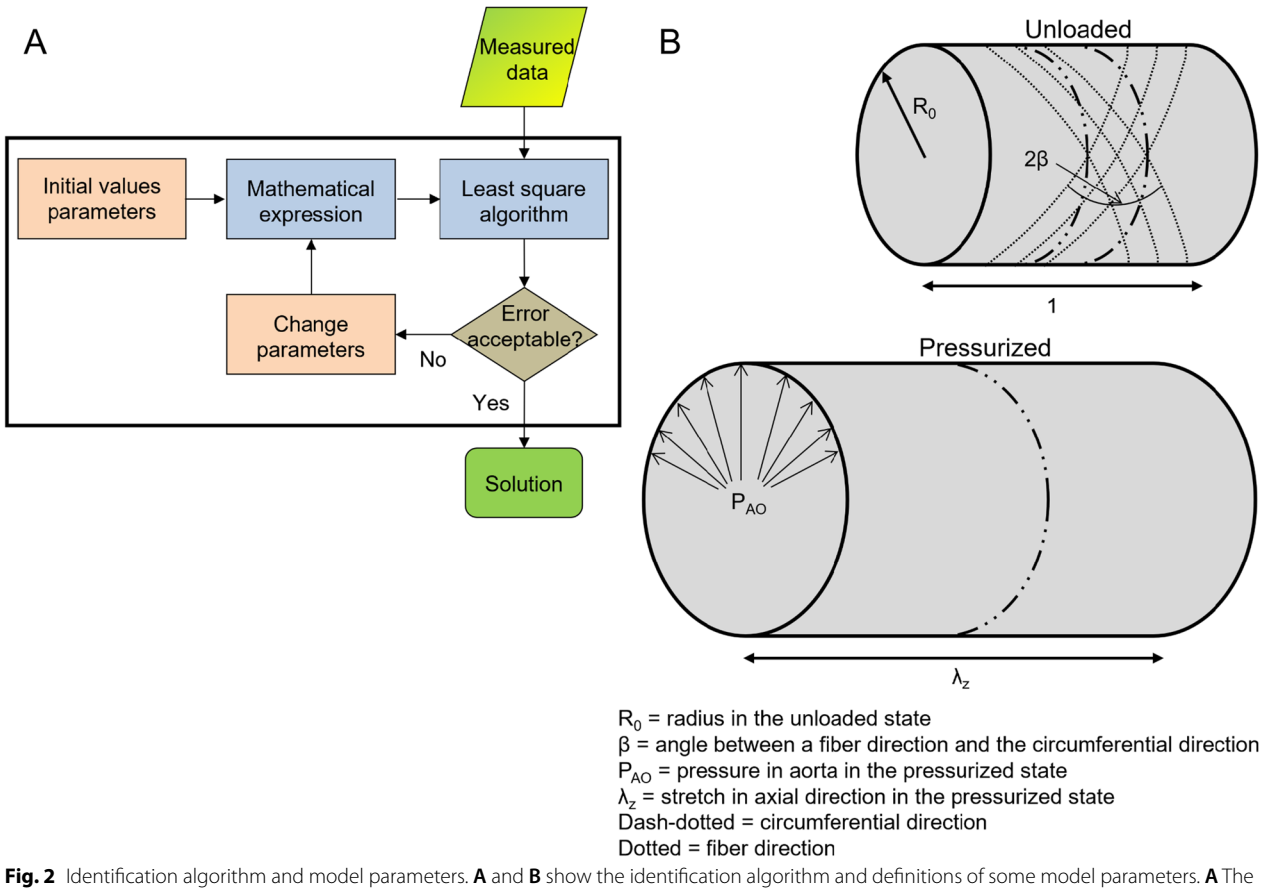

Fig. 2 Identification algorithm and model parameters. **A** and **B** show the identification algorithm and definitions of some model parameters. **A** The identification algorithm used to compute the material parameters in the abdominal aorta, see text for description. **B** An overview of how model parameters β, R_0 and λ_z are defined. The upper cylinder represents the unloaded state with unit length; the lower cylinder represents the pressurized state

- c (Pa)—relates to the stiffness of the isotropic constituents in the vascular wall, mainly elastin.
- k_1 (Pa)—relates to the stiffness of the anisotropic constituents in the vascular wall, mainly collagen.
- k_2 (dimensionless)—reflects the crimpling or folding, cross-linking and entanglement of collagen.
- β (°)—the angle between the circumferential direction and the principal (mean) fiber direction in the unloaded configuration (Fig. 2B).
- R_0 (mm)—the radius in a stress and stretch free (ex situ) unloaded configuration (Fig. 2B)
- λ_z (dimensionless)—longitudinal stretch between the in situ configuration and the (ex situ) unloaded configuration (Fig. 2B).

Values for identified parameters are found in Table 4 in Appendix.

A single stiffness constant, e.g., Young's modulus, cannot accurately predict arterial wall stress [16]. It must be computed from the observed deformation using a set of (nonlinear) equations and associated material parameters [8, 17]. The model used herein is based on a standard Holzapfel–Gasser–Ogden (HGO) nonlinear material model with a neo-Hookean matrix reinforced by a two-family fiber structure [12]. The stress–stretch curve in the circumferential direction can be described by:

$$\begin{aligned}\sigma_\theta = \lambda_\theta \frac{\partial \psi}{\partial \lambda_\theta} &= \sigma_\theta^{\text{iso}} + \sigma_\theta^{\text{aniso}} \\ &= 2C\left[\lambda_\theta^2 - \frac{1}{(\lambda_\theta \lambda_z)^2}\right] + 4k_1(I-1)e^{k_2(I-1)^2}\lambda_\theta \cos^2\beta\end{aligned} \tag{1}$$

where c, k_1, $k_2 > 0$ guarantee energy dissipation and $I = \lambda_\theta^2 \cos^2\beta + \lambda_z^2 \sin^2\beta$ with $\lambda_\theta = \frac{R_0}{r_0}\frac{4\pi r_0^2 + A}{4\pi R_0^2 + \lambda_z A}$. Computed circumferential stress with the result from the identification routine is illustrated in Fig. 1B.

For our purpose, incremental stiffness for a nonlinear material such as biological tissue can be estimated from the slope of the nonlinear stress–stretch curve. This corresponds to the partial derivative of stress with respect to stretch. Hence, there will be two direct stiffnesses and two cross-coupled stiffnesses:

$$S_{\theta\theta} = \frac{\partial \sigma_\theta}{\partial \lambda_\theta}, S_{\theta z} = \frac{\partial \sigma_\theta}{\partial \lambda_z}, S_{z\theta} = \frac{\partial \sigma_z}{\partial \lambda_\theta}, S_{zz} = \frac{\partial \sigma_z}{\partial \lambda_z} \tag{2}$$

where $S_{\theta\theta}$ and $S_{\theta z}$ are circumferential direct and cross-coupled stiffnesses while S_{zz} and $S_{z\theta}$ are longitudinal direct and cross-coupled stiffnesses. Cross-coupled stiffness carries information of how stress in one direction is affected when the artery is stretched in another direction. Thus, $S_{\theta z}$ represents how circumferential stress varies when the vessel wall is stretched in the longitudinal direction and $S_{z\theta}$ represents how longitudinal stress varies when the vessel wall is stretched in the circumferential direction.

3.3 Computed Variables

In the parameter identification routine, the material parameters were computed (c, k_1, k_2 and β) as well as the geometry for the unloaded state (R_0, λ_z). Circumferential stretch (λ_θ) was approximated with $\lambda_\theta = r/R_0$ where r was measured radius and R_0 was identified through the parameter identification process [8]. Furthermore, the circumferential (σ_θ) and longitudinal (σ_z) stresses were computed. Stiffness was computed as the partial derivative of stress with respect to stretch according to Eq. 2; thus, there were four different stiffnesses computed: circumferential direct ($S_{\theta\theta}$) and cross-coupled ($S_{\theta z}$) as well as longitudinal direct (S_{zz}) and cross-coupled ($S_{z\theta}$) stiffnesses.

Mean arterial pressure (MAP) was calculated as $1/3 \times (\text{SBP} - \text{DBP}) + \text{DBP}$, unit Pa. To convert Pa to mmHg, 1 mmHg = 133.32 Pa, was used.

Pressure, radius, circumferential and longitudinal stretch, stress and stiffness were calculated at SBP, DBP and MAP. Notice that the identified parameters are constant during one heartbeat and are not subject to different values at different pressures.

3.4 Linearization

A small amplitude perturbation analysis has been carried out to determine how cross-coupled stiffness manifests through stress. It was done through a linearization close to a point of interest (systolic blood pressure). The linearization follows standard procedures and is a first order Taylor expansion close to the point of interest [18]. For the present study, the linearization will be two dimensional (2D):

$$\begin{pmatrix} \sigma_\theta^{\text{L}}(\lambda_\theta, \lambda_z) \\ \sigma_z^{\text{L}}(\lambda_\theta, \lambda_z) \end{pmatrix} = \begin{pmatrix} \sigma_\theta^0 \\ \sigma_z^0 \end{pmatrix} + \begin{pmatrix} S_{\theta\theta}^0 & S_{\theta z}^0 \\ S_{z\theta}^0 & S_{zz}^0 \end{pmatrix} \begin{pmatrix} \lambda_\theta - \lambda_\theta^0 \\ \lambda_z - \lambda_z^0 \end{pmatrix} \tag{3}$$

Here σ_θ^{L} and σ_z^{L} are the linearized functions while σ_θ and σ_z are the nonlinear functions. $S_{\theta\theta}$, $S_{\theta z}$, $S_{z\theta}$ and S_{zz} are the first partial derivatives of σ_θ, and σ_z with respect to λ_θ and λ_z. λ_θ^0 and λ_z^0 denote the point of interest and superscript "0" serves as a marker for a function calculated at the point of interest.

The linearized functions were used to quantify the influence of stretches on stress through direct and cross-coupled stiffness. By changing the stretch a small amount, q ($0 < q \leq 0.03$) and taking the ratio between the change ($\sigma_i^{\text{L},jq}$) and the original (σ_i^{L}) values, the effect of the change in stretch can be analyzed. Choosing a too large value for q will end up in calculations outside the

validity of the linearization. The higher the ratio, the more impact will stretch have on stress. Four ratios were calculated.

$$R_{ij} = \frac{\sigma_i^{\mathrm{L},jq} - \sigma_i^{\mathrm{L}}}{\sigma_i^{\mathrm{L}}} \quad (i,j = \theta \text{ or } z) \tag{4}$$

with

$$\sigma_i^{\mathrm{L},jq} - \sigma_i^{\mathrm{L}} = S_{ij}^0 \times \lambda_j \times q \quad (i,j = \theta \text{ or } z) \tag{5}$$

Here superscript "q" denotes stress where stretch has been changed a small amount; i and j denote θ or z. The ratios express:

- $R_{\theta\theta}$: circumferential (θ) stretch impact on circumferential (θ) stress
- $R_{\theta z}$: longitudinal (z) stretch impact on circumferential (θ) stress
- $R_{z\theta}$: circumferential (θ) stretch impact on longitudinal (z) stress
- R_{zz}: longitudinal (z) stretch impact on longitudinal (z) stress

The ratios from Eq. (4) were used to assess the influence of stretch on stress via direct stiffness or cross-coupled stiffness.

The impact of stiffness on stress without the effect of stretch was assessed through the stiffness matrix in linearized Eq. (3). Circumferential direct stiffness ($S_{\theta\theta}$) was the largest of the four stiffnesses. Normalizing the elements with $S_{\theta\theta}$ will produce relative values which can be compared within the matrix as well as between different points of interest:

$$nS_{ij}^0 = \frac{S_{ij}^0}{S_{\theta\theta}^0} \quad (i,j = \theta \text{ or } z) \tag{6}$$

The matrix in Eq. (3) can be rewritten as:

$$S_{\theta\theta}^0 \times \begin{pmatrix} 1 & nS_{\theta z}^0 \\ nS_{z\theta}^0 & nS_{zz}^0 \end{pmatrix} \tag{7}$$

Here "n" denotes normalized values. The normalized values express stiffness in terms of $S_{\theta\theta}$; thus, the normalized matrix element for circumferential direct stiffness will always be 1. Since $S_{\theta\theta}$ is largest, the other three stiffnesses will always be less than one.

3.5 Statistics

Arithmetic mean and standard deviation (SD) were calculated for all variables and are expressed as mean ± SD, if not otherwise stated. Variable values calculated at SBP and DBP were regarded as maximum and minimum. A two-way ANOVA test with complementing general linear models was used to compare sex and age groups as suggested by Field [19]. Bonferroni correction was used when multiple comparisons were performed. All parameters were assessed for dependency of age within each sex with a linear regression analysis with Pearson correlation coefficient (R^2). $P < 0.05$ was considered significant in the ANOVA and general linear model as well as in the linear regression analysis. Significance testing is used for a descriptive purpose.

3.6 Software

MATLAB (The Mathwork, Natick, MA, US) version 8.4 (R2014b) was used for computation. IBM SPSS Statistics Version 27 (IBM Corporation, Somers, NY, US) was used for statistical analysis.

4 Results

4.1 Aortic Blood Pressure and Vessel Diameter

Baseline clinical data for the study population are found in Table 1, while abdominal aortic (AA) diameters and blood pressures are shown in Table 2. In males, elderly compared with young had a higher systolic blood pressure (SBP) value, larger AA diameter, but smaller ΔD ($P < 0.05$). Elderly compared with young males appeared

Table 1 Characteristics of the studied population

	Male			Female		
	Young ($n = 5$)	Middle ($n = 5$)	Elderly ($n = 5$)	Young ($n = 5$)	Middle ($n = 5$)	Elderly ($n = 5$)
Age, year	24.8 ± 2.0	47.6 ± 5.6	69.6 ± 1.6	25.4 ± 2.8	49.2 ± 3.1	68.8 ± 2.0
Height, cm	177 ± 8.9	178 ± 6.7	182 ± 4.5[C]	171 ± 8.9	170 ± 4.5	168 ± 4.5
Weight, kg	71.4 ± 8.7[a]	84.8 ± 8.9[B]	87.2 ± 12.3[C]	59.0 ± 9.4	67.0 ± 9.6	64.6 ± 8.0
BMI, kg/m^2	22.6 ± 0.9[a,A]	26.8 ± 2.3	26.3 ± 2.4	20.1 ± 2.0	23.2 ± 4.2	22.8 ± 2.4
BSA, m^2	1.88 ± 0.18	2.03 ± 0.1[B]	2.08 ± 0.2[C]	1.69 ± 0.18	1.78 ± 0.09	1.74 ± 0.1

Data are presented as mean ± SD

BMI body mass index, *BSA* body surface area. Young: 23–30 yr, middle 41–54 yr, elderly 67–72 yr

[a] $P < 0.05$ when comparing young vs elderly for male. [A, B, C] $P < 0.05$ when comparing male vs female for young, middle and elderly, respectively

Table 2 Abdominal aortic pressure and diameter

	Male			Female		
	Young	Middle	Eldelry	Young	Middle	Eldelry
SBP, mmHg	114 ± 12^{a}	133 ± 18	135 ± 22	119 ± 14	123 ± 10	126 ± 15
DBP, mmHg	62 ± 8	71 ± 6	70 ± 12	66 ± 9	66 ± 7	64 ± 5
MAP, mmHg	$79 \pm 9^{(a)}$	92 ± 8	92 ± 15	84 ± 11	85 ± 7	85 ± 8
PP, mmHg	$52 \pm 5^{(a)}$	62 ± 17	65 ± 15	52 ± 5	57 ± 6	62 ± 12
Diameter SBP, mm	$15.9 \pm 1.2^{aa,bb}$	19.4 ± 1.2^{BB}	20.5 ± 2.1^{CC}	15.1 ± 0.8^{a}	16.3 ± 0.7	17.2 ± 2.4
Diameter DBP, mm	$13.8 \pm 1.4^{aa,bb}$	18.2 ± 1.4^{BB}	19.8 ± 2.2^{CC}	13.3 ± 1.4^{aa}	15.0 ± 1.2	16.6 ± 2.4
Δ Diameter, mm	$2.14 \pm 0.32^{aa,bb}$	1.14 ± 0.47	0.77 ± 0.25	1.79 ± 0.75^{a}	1.28 ± 0.45^{c}	0.67 ± 0.08

Data are presented as mean ± SD

SBP systolic blood pressure, *DBP* diastolic blood pressure, *MAP* mean arterial pressure, *PP* pulse pressure, *Diameter SBP* diameter at systolic blood pressure, *Diameter DBP* diameter at diastolic blood pressure, *Δ Diameter* diameter SBP − diameter DBP

$^{a, b, c}$ $P < 0.05$ when comparing young vs elderly, young vs middle, middle vs elderly, respectively, for male or female; $^{aa, bb}P < 0.01$. $^{BB, CC}P < 0.01$ when comparing male vs female for middle and elderly, respectively. '( )' indicate $P < 0.10$

to have a higher mean arterial pressure (MAP) value ($P = 0.07$) as well as pulse pressure (PP) value ($P = 0.08$). In females, elderly compared with young had larger AA diameters, but smaller ΔD than ($P < 0.05$). Males compared to females had larger AA diameters ($P < 0.05$). Changes in the pulsatile diameter of the AA (ΔD) and blood pressure did not differ by sex.

4.2 Linear Model

For the linearization, the groups of elder and middle aged were combined to one group ($n = 20$) of males ($n = 10$) and females. This unified group was investigated, and results are reported in Fig. 3.

4.2.1 Comparing Normalized Linear Model Stiffness Matrix Elements ($nS_{\theta\theta}$, $nS_{\theta z}$, $nS_{z\theta}$, nS_{zz}) at SBP, DBP and MAP

At SBP in males and females, $nS_{\theta\theta}$ had a 70–100% higher value compared with $nS_{\theta z}$, $nS_{z\theta}$ and nS_{zz} (males: 1.00 ± 0.00 vs. 0.59 ± 0.05 vs. 0.51 ± 0.03 vs. 0.56 ± 0.10, respectively, $P < 0.01$, and females: 1.00 ± 0.00 vs. 0.57 ± 0.06 vs. 0.51 ± 0.04 vs. 0.57 ± 0.12, respectively, $P < 0.01$). In males and females, there were no differences when comparing $nS_{\theta z}$, $nS_{z\theta}$ and nS_{zz} (Fig. 3A).

4.2.2 Comparing Ratio of Stresses ($R_{\theta\theta}$, $R_{\theta z}$, $R_{\theta z}$, R_{zz}) at SBP, i.e., Combined Effect of Stiffness and Stretch on Stress

At SBP in males, $R_{\theta\theta}$ had a higher value compared with $R_{\theta z}$ while $R_{\theta z}$ had a lower value compared to $R_{z\theta}$ and R_{zz}, (0.053 ± 0.027 vs. 0.027 ± 0.013 vs. 0.047 ± 0.023 vs. 0.048 ± 0.019, respectively, $P < 0.05$). In females, $R_{\theta\theta}$ had a higher value compared with $R_{\theta z}$ (0.045 ± 0.020 vs. 0.023 ± 0.010, $P < 0.05$), while $R_{\theta z}$ appeared to be lower than $R_{z\theta}$ and R_{zz}, (0.040 ± 0.017 vs. 0.040 ± 0.015, respectively, $P < 0.1$). At SBP in males and females, $R_{\theta\theta}$ was almost 100% higher compared to $R_{\theta z}$, and when comparing $R_{\theta\theta}$, $R_{z\theta}$ and R_{zz}, all three were of the same magnitude (Fig. 3B).

Figure 3A shows the impact of stiffness on stress, while Fig. 3B includes stretch and thus shows the combined effect of stiffness and stretch on stress. λ_θ had a higher value compared to longitudinal stretch λ_z (Table 3). The effect of this difference is not seen in Fig. 3A but is considered in Fig. 3B. Comparing Fig. 3A and B expose the impact of stiffness and stretch on stress. First, $S_{\theta z}$ and $S_{z\theta}$ were of the same magnitude. Second, combining $S_{\theta z}$ and $S_{z\theta}$ with respective λ_θ and λ_z showed that a small change in λ_z will have a lesser effect on circumferential stress (second bar from left in Fig. 3B) compared to the effect a small change in λ_θ will have on longitudinal stress (third bar from left in Fig. 3B). Hence, it appears that the effect of a change in λ_θ will have a greater impact on longitudinal stress than a change in λ_z will have on circumferential stress.

4.3 Aortic Wall Stiffness and Stretch

Stiffness and stretch are reported in Table 3.

4.3.1 Comparing Stiffness ($S_{\theta\theta}$, $S_{\theta z}$, $S_{z\theta}$, S_{zz}) Between Age Groups Within a Sex at SBP, DBP and MAP

(From left to right in Table 3).

At SBP, DBP and MAP, in males, elderly and middle aged compared with young had a higher $S_{\theta\theta}$, $S_{\theta z}$, $S_{z\theta}$ and S_{zz} ($P < 0.05$, respectively). In females, elderly compared with young had a higher $S_{\theta\theta}$, $S_{\theta z}$ and $S_{z\theta}$ ($P < 0.05$, respectively); there appeared to be a higher S_{zz} for elderly when compared to young ($P < 0.1$).

At SBP, DBP and MAP, in males, $S_{\theta\theta}$, $S_{\theta z}$, $S_{z\theta}$ and S_{zz} correlated positively with age ($P < 0.05$, respectively). This holds true for females as well ($P < 0.05$, respectively),

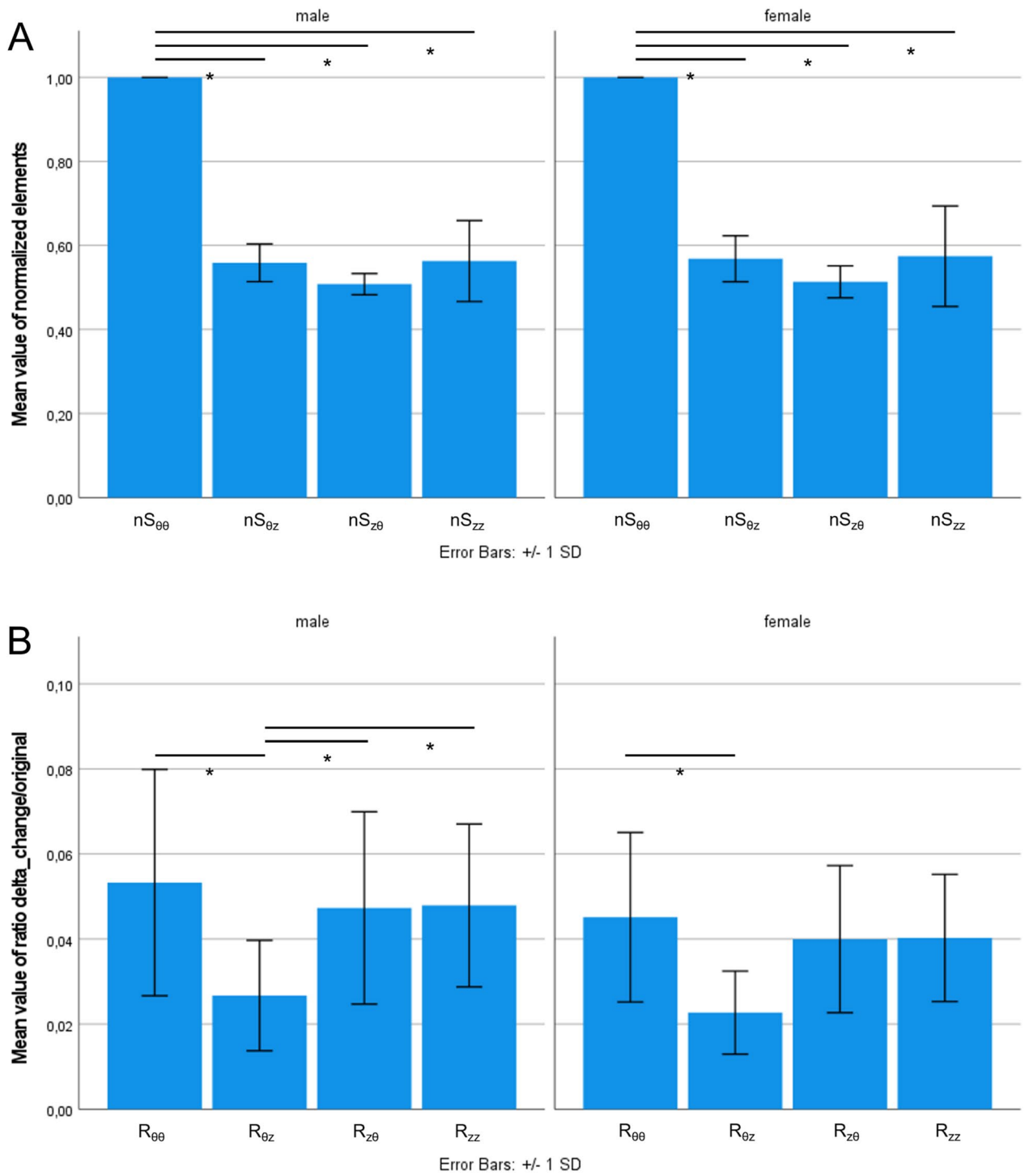

Fig. 3 Linearized stiffness matrix at SBP, elderly and middle-aged group. Results from linearization at SBP. Normalized linear model stiffness matrix (**A**) and ratio between the change and the original values (**B**) for males (left) and females (right) at SBP in the elderly and middle-aged group. Panel A reveals the impact of stiffness alone on stress, while panel B include stretch and thus show the combined effect of stiffness and stretch on stress. There were no differences between sexes. $nS_{\theta\theta}$ had a higher value compared to $nS_{\theta z}$, $nS_{z\theta}$ and nS_{zz}, which, on the other hand, were of the same magnitude. In males, $R_{\theta z}$ had a lower value compared to $R_{\theta\theta}$, $R_{z\theta}$ and R_{zz} which, in turn, were of the same magnitude. In females, $R_{\theta z}$ was lower compared to $R_{\theta\theta}$, and appeared to be lower compared to $R_{z\theta}$ and R_{zz} which, in turn were of the same magnitude. Error bars ± 1 SD.

Table 3 Stiffness and stretch at different blood pressures for sexes, divided into age groups

	Male					Female				
	Young ($n=5$)	**Middle ($n=5$)**	**Elderly ($n=5$)**	**Total**	**Regr (R^2)**	**Young ($n=5$)**	**Middle ($n=5$)**	**Elderly ($n=5$)**	**Total**	**Regr (R^2)**
SBP										
$S_{\theta\theta}$ (MN/m)	$1.02 \pm 0.48^{aa, b}$	4.12 ± 3.13	5.49 ± 2.51	$3.54 \pm 2.90^{(*), €€, ££}$	0.49 ↑↑	1.38 ± 0.71^{a}	$2.15 \pm 1.15^{(c)}$	4.25 ± 2.13	$2.60 \pm 1.84^{€€, ££}$	0.38 ↑
$S_{\theta z}$ (MN/m)	$0.66 \pm 0.32^{aa, b}$	2.34 ± 1.78	2.94 ± 1.31	$1.98 \pm 1.56^{(*), €€, ££}$	0.45 ↑↑	0.88 ± 0.49^{a}	1.33 ± 0.72	2.24 ± 1.16	$1.48 \pm 0.97^{€€, ££}$	0.30 ↑
$S_{z\theta}$ (MN/m)	$0.53 \pm 0.27^{aa, b}$	2.13 ± 1.67	2.76 ± 1.25	$1.81 \pm 1.49^{(*), €€, ££}$	0.47 ↑↑	0.74 ± 0.44^{a}	1.19 ± 0.70	2.09 ± 0.70	$1.34 \pm 0.94^{€€, ££}$	0.32 ↑
S_{zz} (MN/m)	$0.77 \pm 0.30^{aa, b}$	2.16 ± 1.27	2.84 ± 1.11	$1.92 \pm 1.28^{€, £}$	0.53 ↑↑	$1.01 \pm 0.51^{(a)}$	1.45 ± 0.76	2.10 ± 1.08	$1.49 \pm 0.72^{(€), (£)}$	0.20 ↗
λ_θ	$1.28 \pm 0.06^{aa, bb}$	$1.19 \pm 0.14^{(c)}$	1.09 ± 0.03	$1.22 \pm 0.15^{€}$	0.74 ↓↓	$1.33 \pm 0.13^{aa, b}$	1.20 ± 0.08	1.12 ± 0.03	$1.21 \pm 0.12^{€}$	0.56 ↓↓
λ_z [§]	$1.050 \pm 0.005^{aa, (b)}$	$1.029 \pm 0.001^{(c)}$	1.012 ± 0.003	1.03 ± 0.02	0.66 ↓↓	$1.049 \pm 0.026^{aa, bb}$	1.027 ± 0.010	1.018 ± 0.006	1.03 ± 0.02	0.44 ↓↓
DBP										
$S_{\theta\theta}$ (MN/m)	$0.43 \pm 0.13^{aa, b}$	$1.24 \pm 0.61^{(c)}$	$1.80 \pm 0.72^{(C)}$	1.16 ± 0.78	0.59 ↑↑	0.58 ± 0.26^{a}	0.82 ± 0.39	1.24 ± 0.56	0.88 ± 0.48	0.29 ↑
$S_{\theta z}$ (MN/m)	$0.22 \pm 0.06^{aa, b}$	$0.59 \pm 0.30^{(c)}$	$0.86 \pm 0.35^{(C)}$	0.56 ± 0.37	0.57 ↑↑	0.28 ± 0.12^{a}	0.38 ± 0.18	0.59 ± 0.26	0.41 ± 0.22	0.28 ↑
$S_{z\theta}$ (MN/m)	$0.20 \pm 0.05^{aa, b}$	$0.56 \pm 0.30^{(c)}$	$0.83 \pm 0.34^{(C)}$	0.53 ± 0.36	0.58 ↑↑	0.26 ± 0.11^{a}	0.36 ± 0.17	0.57 ± 0.27	0.39 ± 0.22	0.30 ↑
S_{zz} (MN/m)	$0.41 \pm 0.11^{aa, b}$	$1.12 \pm 0.53^{(c)}$	$1.68 \pm 0.59^{(C)}$	1.07 ± 0.69	0.65 ↑↑	$0.55 \pm 0.23^{(a)}$	0.79 ± 0.40	1.11 ± 0.59	0.82 ± 0.47	0.22 ↗
λ_θ	$1.19 \pm 0.03^{aa, b}$	1.12 ± 0.09^{c}	1.05 ± 0.02	1.12 ± 0.08	0.63 ↓↓	$1.16 \pm 0.05^{aa, (b)}$	1.10 ± 0.04	1.07 ± 0.02	1.11 ± 0.05	0.57 ↓↓
λ_z [§]	$1.050 \pm 0.005^{aa, (b)}$	$1.029 \pm 0.001^{(c)}$	1.012 ± 0.003	1.03 ± 0.02	0.66 ↓↓	$1.049 \pm 0.026^{aa, bb}$	1.027 ± 0.010	1.018 ± 0.006	1.03 ± 0.02	0.44 ↓↓
MAP										
$S_{\theta\theta}$ (MN/m)	$0.51 \pm 0.17^{aa, b}$	$1.40 \pm 0.67^{(c)}$	2.10 ± 1.12	1.34 ± 0.98	0.50 ↑↑	0.67 ± 0.29^{a}	0.88 ± 0.36	1.53 ± 0.59	1.03 ± 0.55	0.38 ↑
$S_{\theta z}$ (MN/m)	$0.27 \pm 0.09^{aa, b}$	$0.68 \pm 0.33^{(c)}$	1.02 ± 0.56	0.66 ± 0.47	0.68 ↑↑	0.34 ± 0.14^{a}	0.42 ± 0.16	0.74 ± 0.28	0.50 ± 0.26	0.36 ↑
$S_{z\theta}$ (MN/m)	$0.24 \pm 0.08^{aa, b}$	$0.64 \pm 0.32^{(c)}$	0.97 ± 0.54	0.62 ± 0.46	0.47 ↑↑	0.30 ± 0.13^{a}	0.39 ± 0.15	0.70 ± 0.28	0.46 ± 0.28	0.38 ↑
S_{zz} (MN/m)	$0.46 \pm 0.13^{aa, b}$	$0.18 \pm 0.53^{(c)}$	$1.76 \pm 0.68^{(C)}$	1.13 ± 0.99	0.58 ↑↑	$0.60 \pm 0.23^{(a)}$	0.82 ± 0.38	1.19 ± 0.59	0.87 ± 0.47	0.24 ↗
λ_θ	$1.25 \pm 0.04^{aa, b}$	$1.14 \pm 0.11^{(c)}$	1.07 ± 0.02	1.15 ± 0.10	0.69 ↓↓	$1.22 \pm 0.07^{aa, b}$	1.14 ± 0.05	1.14 ± 0.05	1.15 ± 0.08	0.58 ↓↓
λ_z [§]	$1.050 \pm 0.005^{aa, (b)}$	$1.029 \pm 0.001^{(c)}$	1.012 ± 0.003	1.03 ± 0.02	0.66 ↓↓	$1.049 \pm 0.026^{aa, bb}$	1.027 ± 0.010	1.018 ± 0.006	1.03 ± 0.02	0.44 ↓↓

Data are presented as mean ± SD

SBP systolic blood pressure *DBP* diastolic blood pressure, *MAP* mean arterial pressure, $S_{\theta\theta}$ direct stiffness in circumferential direction, $S_{\theta z}$ cross-coupled stiffness in circumferential direction, $S_{z\theta}$ cross-coupled stiffness in longitudinal direction, S_{zz} direct stiffness in longitudinal direction. λ_θ stretch in circumferential direction, λ_z stretch in longitudinal direction. Young: 23–30 years, middle 41–54 years, elderly 67–72 years

[§] λ_z is constant and therefore do not change with pressure. [*] $P < 0.05$ when comparing male vs female independent of age (total), with respect to pressure. [€, £] $P < 0.05$, when comparing pressure (SBP vs DBP, SBP vs MAP, respectively) with respect to male or female. [€€, ££]indicate $P < 0.01$

[a, b, c] $P < 0.05$ when comparing young vs elderly, young vs middle, middle vs elderly, respectively, for male or female. [aa, bb] $P < 0.01$. [C] $P < 0.05$ when comparing male vs female for elderly. '()' indicate $P < 0.10$

↑↑, ↑, ↗: positive correlation; ↓↓, ↓, ↘: negative correlation; triplet from left to right: $P < 0.01$, $P < 0.05$, $P < 0.10$, respectively. → = no correlation

except for S_{zz}, which appeared to correlate positively ($P < 0.1$). Altogether, our findings suggest that $S_{\theta\theta}$, $S_{\theta z}$, $S_{z\theta}$ and S_{zz} increased with age.

Furthermore, elderly compared with young males as well as females showed a higher value at SBP and DBP for $S_{\theta\theta}$, $S_{\theta z}$, $S_{z\theta}$ and S_{zz} (SBP: male 400%, 400%, 350%, 270%, respectively; female 200%, 200%, 150%, 100%, respectively. DBP: male 300%, 300%, 300%, 300%, respectively; female 100%, 100%, 100%, 100%, respectively). Thus, it seems that the increase in stiffness from the young to the elderly was constant and approximately two times higher in males compared with females both at SBP and DBP, i.e., for the physiological pressure range.

For elderly males and females at SBP, $S_{\theta\theta}$ compared with $S_{\theta z}$, $S_{z\theta}$ and S_{zz} had a higher value (90%, 100% and 95–100%, respectively). Hence, independent of sex, the elderly had values where $S_{\theta\theta}$ was approximately twofold higher than $S_{\theta z}$, $S_{z\theta}$ and S_{zz} which, in turn, were of the same magnitude. Independent of sex and pressure, it appears that for the elderly, $S_{\theta z}$ had approximately the same value as $S_{z\theta}$.

4.3.2 Comparing Stiffness Between Sexes Within an Age Group at SBP, DBP and MAP

(From left to right in Table 3).

At DBP, for the elderly, males compared to females appeared to have higher $S_{\theta\theta}$, $S_{\theta z}$, $S_{z\theta}$ and S_{zz} ($P < 0.1$).

Males compared to females had a lower stiffness as young but a higher stiffness as elderly (Table 3). This suggests two things: first, for the young group, the female abdominal aortic wall may be stiffer compared to that of the male; second: the male abdominal aortic wall grows stiffer at a higher rate with age.

4.3.3 Comparing Stretch (λ_θ, λ_z) Between Age Groups Within a Sex at SBP, DBP and MAP

(From left to right in Table 3).

At SBP, DBP and MAP in both sexes, elderly and middle aged compared with young had a lower λ_θ and λ_z ($P < 0.05$, respectively). In the model, λ_z was assumed to be constant over blood pressure, [8].

At SBP, DBP and MAP in both males and females, λ_θ and λ_z correlated negatively with age ($P < 0.05$, respectively) which suggests that λ_θ and λ_z decreased with age.

From Table 3, it appears that the difference in λ_θ between young and elderly at SBP was approximately the same in males and females although at DBP males expressed a higher difference compared to females.

4.3.4 Comparing Stretch Between Sexes Within an Age Group at SBP, DBP and MAP

(From left to right in Table 3).

Males compared with females showed no statistically significant difference in λ_θ and λ_z.

5 Discussion

The main findings of this study were as follows:

1. The effect of a change in circumferential stretch appeared to have a greater impact on longitudinal stress than a change in longitudinal stretch might have on circumferential stress.
2. Circumferential and longitudinal direct and cross-coupled stiffnesses increased while circumferential and longitudinal stretches decreased with age, independent of sex.
3. For the young group, the female abdominal aortic wall is stiffer compared to that of the male while for the elderly group the male abdominal aortic wall seemed to be stiffer than the female wall.

The mechanical forces maintain a balance in the vascular wall through remodeling. A stretch of the vessel wall will cause an increased wall stress. The magnitude of the stress will be determined by the wall stiffness. Biological material such as vascular tissue will have a nonlinear stress–stretch relationship, meaning that the stiffness is nonlinear. Not only shear, circumferential and longitudinal stresses are fundamental mechanical properties in arterial wall remodeling, but the interdependency of circumferential–longitudinal coupling of stresses and stretches is considered to be of importance as well [4, 5, 20].

Our results suggest that cross-coupled stiffness participates in the interdependency between circumferential and longitudinal coupling of stresses and stretches. In independent processes, we propose that an increase in stretch in the circumferential direction affects longitudinal stress through cross-coupled circumferential stiffness and the axial force with longitudinal stretch affects circumferential stress through longitudinal cross-coupled stiffness. Interdependency between circumferential and longitudinal remodeling has been shown where a longitudinally stretched vessel grew into its new length recovering a prestretched stress value, while wall thickness increased but not circumferential stress [21]. Increased cell proliferation of smooth muscle and endothelial cells as well as increased internal elastic laminae fenestrae

size, but not density was reported [21]. Increase in wall thickness is a reversible process [22]. An increase in vessel length is not reversible since matrix metalloproteinase (MMP) activity degrades proteins and prevents longitudinal strain from returning to normal values [23].

The effect of a change in circumferential stretch appears to have a greater impact on longitudinal stress than a change in longitudinal stretch might have on circumferential stress. The linearized model showed that an increase in longitudinal stress was composed by approximately 50% of stress depending on cross-coupled stiffness while an increase in circumferential stress was composed by approximately 33% of stress derived from cross-coupled stiffness. This suggests that circumferential stretch may have a significant impact on longitudinal remodeling while longitudinal stretch probably has a minor impact on circumferential remodeling.

The blood pressure-induced alterations of circumferential stretch may, through the proposed mechanism of cross-coupled stiffness, contribute significantly to increased longitudinal stress and stretch, resulting in the aorta growing into its new length. Considering that decreased longitudinal strain might exacerbate a lengthening and create tortuosity [23], there are two different mechanisms working together in an unfavorable way with respect to optimal aortic length. This may, at least in part, offer an explanation to why the aorta is prone to tortuosity.

It is well accepted that a stiffer arterial wall is accompanied by a higher blood pressure, e.g., hypertension [24]. In this context, stiffness is commonly associated with circumferential stiffness. The role of longitudinal stiffness in hypertension is much less investigated as well as cross-coupled stiffness. Our findings suggest that with increasing age, circumferential stiffness gets proportionally higher compared to longitudinal and cross-coupled stiffness while longitudinal and cross-coupled stiffnesses are of the same magnitude. This indicates that the composition of the vessel wall is changed in a stiffer direction by way of loadbearing structures in circumferential and longitudinal directions as well as the interdependency of the circumferential–longitudinal coupling.

Abdominal aortic aneurysms can have complicated geometries and aneurysm diameter is mainly governed by shear stress. Aneurysms rupture when wall stress exceeds wall strength [25]. Under pathological circumstances, direct and cross-coupled stiffness may adopt quite different values compared to ordinary conditions. However, our findings suggest that in an adverse situation, longitudinal stretch could contribute to circumferential stress exceeding wall strength resulting in wall rupture, even though the aneurysmatic diameter is small and/or the presence of a small circumferential stretch.

Our finding of an age-dependent increase in circumferential and longitudinal stiffness as well as decrease in stretch is in accordance with the literature, although we cannot show a difference between sexes in stretch [14, 24]. Furthermore, this age-dependent increase in circumferential stiffness agrees with previous reported findings [10].

For the young group, the female abdominal aortic wall may be stiffer compared to that of the male while for the elderly group the male abdominal aortic wall seems to be stiffer than in the female, indicating that the male abdominal aortic wall may grow stiffer at a higher rate with age. The gain in male abdominal aortic wall stiffness with age is in accordance with observations of a more accelerated ageing process in the aorta in males compared to females [26]. Female sex hormones seem to protect against aortic wall elastolysis, which in turn will contribute to vessel wall stiffening [27]. The effect of postmenopausal hormone replacement therapy in females seems to reduce arterial stiffness [28] further suggesting that females are better protected against aortic wall stiffening than males.

Different mechanisms contribute to the age-related alterations of the vascular wall. Increased wall stress has been suggested to induce synthesis of collagen in the fiber direction and thus a maintained stretch of the individual fibers [11, 29, 30]. The orientation of collagen fibers may also be important since it has been found to be more helical in the media and more longitudinal in the adventitia [31, 32]. Additionally, increased glycation of elastin and collagen as well as changed isoforms of collagen in the aortic wall might contribute to the age-related increase in stiffness [33].

It has been pointed out that constitutive equations describing biological material such as the arterial vessel wall suggest a circumferential–longitudinal coupling of stresses and stretches [5, 17, 20]. Our model expresses such an interdependency with a circumferential–longitudinal coupling where both circumferential and longitudinal stresses depend on stretch in circumferential and longitudinal directions ($\sigma_\theta(\lambda_\theta, \lambda_z)$ and $\sigma_z(\lambda_\theta, \lambda_z)$) [8]. An attempt to quantify this interdependency was made through a linearization of the model equations. To the authors knowledge, there has been no in vivo quantification of the remodeling characteristics in one direction caused by stretching in cross-directions. Biaxial tests ex vivo provide some information regarding the interconnection of forces. Nevertheless, as a tool for assessing in vivo mechanisms, PIMMP may be used to explore mechanical properties of the vessel wall and may serve as a potential tool for risk assessment for the development of cardiovascular disease.

Based on our results, we propose that cross-coupled stiffness may play a part in the age-related remodeling of the aortic wall, where an increase in circumferential cross-coupled stiffness induced longitudinal stress constitute 50% of the change in total longitudinal stress and therefore may contribute to aortic tortuosity. Furthermore, with increasing age it seems that the interdependency of circumferential–longitudinal coupling increases possibly due to a change in composition of the aortic wall which may be a contributing factor in hypertension. Additionally, under adverse conditions our findings indicate that, e.g., a longitudinal stretch could contribute to circumferential stress increasing the likelihood of aneurysm rupture.

6 Limitations

Since there are differences between different parts of the vascular system and the abdominal aorta as well as between different segments of the aorta, with respect to histology and pulse-wave velocity, it must be emphasized that our findings should be extrapolated with caution to other segments of the aorta. Furthermore, assumptions in the model can affect the use of PIMMP.

The parameter identification algorithm with the attendant mechanical model was validated against finite element (FE) models of an artery, a procedure which is also known as "in silico" validation. The validation showed good agreement between PIMMP and the FE models [9]. In particular, the longitudinal response in the simulation is sensitive to the longitudinal prestretch (λ_z), and thus, this parameter is a natural candidate for the validation procedure. The PIMMP result shows a longitudinal prestretch within the range which has been reported from autopsy study of the human abdominal aorta [14]. In general, nonlinear arterial models are difficult to validate experimentally since each model parameter needs to be changed independently of the other parameters. Therefore, our model has not been validated against measurements in vivo.

The strain–energy function used in this study is based on Holzapfel et al. [12] (Eq. 10). Compared to Schulze-Bauer and Holzapfel [7], it allows for a better fit to young subjects, particularly in the low-pressure region where the mechanical behavior is primarily determined by isotropic material components such as elastin and the collagen recruitment is small [8].

The mechanical model is based on an assumption of the cylindrical wall being a membrane, i.e., wall thickness should be negligible when compared with the radius. However, wall thickness-to-radius ratio is ~ 0.1–0.2 for the abdominal aorta; therefore, the validity of the assumption might be argued [11]. Furthermore, the aortic wall consists of three distinct layers which all have different mechanical properties [34]. An exact model should consider this. However, such a high resolution in the model might introduce dependencies among the parameters during parameter identification [15]. Regarding the parameters from the membrane model as averages, it might be thought of as describing the global response of the three layers of the aortic wall.

Our model concerns the passive mechanical properties of the aorta and assumes that the outer boundary is traction free, i.e., the artery is a freestanding tube with neglected periadventitial support. It has been shown that the difference in circumferential stress between the freestanding and the tethered states is small, approximately 10% [35]. Considering the limited effect of tethering and that such mechanism would require the identification of the mechanical properties of surrounding tissue, we decided that a freestanding approach would be sufficient for this study.

7 Conclusion

This paper presents quantitative estimates for circumferential direct and cross-coupled as well as longitudinal direct and cross-coupled stiffnesses for the human abdominal aorta stratified for age and sex, based on in vivo and in situ measured radius and pressure. These stiffnesses have so far only been quantified through measurements ex vivo, ex situ in the laboratory. Our findings of an age-related circumferential remodeling acting through cross-coupled stiffness might have a major impact on longitudinal stress and remodeling and possibly aortic tortuosity. The findings suggest an age-related change in wall constituents. A potential explanation, although not studied here, could be related to chemical alterations of wall constituents and changes in the physical distribution of fibers.

Appendix

The Identification of Model Parameters and the Mechanical Model

Using measured pressure and diameter, membrane stress can be computed according to Laplace law in both circumferential and longitudinal directions [8]:

$$\sigma_\theta^{lp} = \frac{4\pi r_0^2 + A}{2A}\mathrm{P}, \sigma_z^{lp} = \frac{\pi r_0^2 P + F}{A} \tag{8}$$

where r_0 is the inner radius of the artery in its physiological state, A is the cross-sectional area, P is the pressure and F is the in situ axial force. Laplace law in Eq. (8) is rewritten so that wall thickness is estimated through inner radius and cross-sectional area.

Table 4 Model parameters

	c (kPa)	k_1 (kPa)	k_2 (–)	β (°)	R_0 (mm)	λ_z (–)
Male	131.50 ± 90.00	14.18 ± 20.94	196.76 ± 264.22	42.38 ± 4.38	7.80 ± 1.78	1.03 ± 0.02
Female	101.65 ± 63.75	8.64 ± 10.00	134.95 ± 175.15	42.31 ± 3.82	6.77 ± 1.23	1.03 ± 0.02

Data are presented as mean ± SD

Inner radius is measured, and cross-sectional area is calculated as: males: $A = 19.60 + 0.80 \times \text{age}$, females: $A = 20.52 + 0.56 \times \text{age}$; age in years and A in mm^2, following Åstrand et al. [10, 11].

The computation requires that axial force is constant and independent of the internal pressure while the ratio between the longitudinal and circumferential stresses is known at one internal pressure P. Assuming the stress ratio taken to be $\gamma = \sigma_z/\sigma_\theta = 0.59$ at $P = 13.3$ kPa, the axial force can be determined explicitly following Schulze-Bauer and Holzapfel [7]. Note that membrane stresses following Laplace law are only functions of the applied load (pressure) and geometry (diameter) and do not depend on the blood vessel's material properties. As a consequence, the membrane stress becomes statically determined [8].

The six model parameters are identified by comparing stresses computed according to Laplace (Eq. 8) which are based on measurement, with stresses from the mechanical model (Eqs. 11 and 12). The process is based on a nonlinear least-square fitting routine using an objective function:

$$\phi(\boldsymbol{\kappa}) = \sum_{n=1}^{N} \left\{ \left[\sigma_\theta(\boldsymbol{\kappa}, r_0, n) - \sigma_\theta^{lp}(\boldsymbol{\kappa}, r_0, n) \right]^2 + \left[\sigma_z(\boldsymbol{\kappa}, r_0, n) - \sigma_z^{lp}(\boldsymbol{\kappa}, r_0, n) \right]^2 \right\} \tag{9}$$

where $\boldsymbol{\kappa} = (R_0, \lambda_z, c, k_1, k_2, \beta)$ is the parameter vector referred to as the model parameters, n is a sample, N is the total number of samples. The model parameters are the solution to the minimization problem:

$$\begin{cases} \min\limits_{\boldsymbol{\kappa}} \phi(\boldsymbol{\kappa}) \\ \text{subject to} : \underline{\boldsymbol{\kappa}} \le \boldsymbol{\kappa} \le \overline{\boldsymbol{\kappa}} \end{cases}$$

where $\underline{\boldsymbol{\kappa}}$ and $\overline{\boldsymbol{\kappa}}$ are the lower and upper boundaries for $\boldsymbol{\kappa}$, respectively.

Identified model parameters agree with results published by Åstrand et al. [10] (Table 4).

An artery is a nonlinear material, and as such, its wall stress cannot be estimated from a single stiffness constant. Arterial wall stress must be computed from an observed deformation using a set of (nonlinear) equations and associated material parameters [8, 17]. Our model is based on a standard Holzapfel–Gasser–Ogden (HGO) nonlinear material model with a neo-Hookean matrix reinforced by a two-family fiber structure with a strain energy function suggested by Holzapfel et al. [12]:

$$\psi = \psi_{\text{iso}} + \psi_{\text{aniso}} = c(I_1 - 3) + \frac{k_I}{k_2}\left(e^{k_2(I-1)^2} - 1\right) \tag{10}$$

where $c, k_1, k_2 > 0$ to guarantee material convexity and the invariants are $I_1 = \lambda_\theta^2 + \lambda_z^2 + \left(\lambda_\theta^2 \lambda_z^2\right)^{-1}$ and $I = \lambda_\theta^2 \cos^2\beta + \lambda_z^2 \sin^2\beta$ with $\lambda_\theta = \frac{R_0}{r_0}\frac{4\pi r_0^2 + A}{4\pi R_0^2 + \lambda_z A}$. The circumferential and longitudinal stresses can be computed as:

$$\begin{aligned} \sigma_\theta &= \lambda_\theta \frac{\partial \psi}{\partial \lambda_\theta} = \sigma_\theta^{\text{iso}} + \sigma_\theta^{\text{aniso}} \\ &= 2C\left[\lambda_\theta^2 - \frac{1}{(\lambda_\theta \lambda_z)^2}\right] + 4k_1(I-1)e^{k_2(I-1)^2}\lambda_\theta \cos^2\beta \end{aligned} \tag{11}$$

$$\begin{aligned} \sigma_z &= \lambda_z \frac{\partial \psi}{\partial \lambda_z} = \sigma_z^{\text{iso}} + \sigma_z^{\text{aniso}} \\ &= 2C\left[\lambda_z^2 - \frac{1}{(\lambda_\theta \lambda_z)^2}\right] + 4k_1(I-1)e^{k_2(I-1)^2}\lambda_z^2 \sin^2\beta \end{aligned} \tag{12}$$

It can be noticed that computed stress consists of isotropic and anisotropic components in both the circumferential and longitudinal directions [8, 10]:

$$\sigma_\theta = \sigma_\theta^{\text{iso}} + \sigma_\theta^{\text{aniso}}, \sigma_z = \sigma_z^{\text{iso}} + \sigma_z^{\text{aniso}}. \tag{13}$$

Isotropy and anisotropy are directional properties linked to the constituent's orientation. Furthermore, they are independent of the material shape and volume. For the vascular wall, the isotropic and anisotropic components primarily reflect structures such as elastin and collagen, respectively [12, 17].

Abbreviations

A: Area; AA: Abdominal aorta; AAA: Abdominal aortic aneurysm; ANOVA: Analysis of variance; D: Diameter; ΔD: Pulsatile diameter, $\Delta D = D@\text{SBP} - D@\text{DBP}$; DBP: Diastolic blood pressure; $S_{\theta\theta}$: Circumferential direct stiffness, $S_{\theta\theta} = \frac{\partial \sigma_\theta}{\partial \lambda_\theta}$; $S_{\theta z}$: Circumferential cross-coupled stiffness, $S_{\theta z} = \frac{\partial \sigma_\theta}{\partial \lambda_z}$; $S_{z\theta}$: Longitudinal cross-coupled stiffness, $S_{z\theta} = \frac{\partial \sigma_z}{\partial \lambda_\theta}$; S_{zz}: Longitudinal direct stiffness, $S_{zz} = \frac{\partial \sigma_z}{\partial \lambda_z}$; ECM: Extracellular matrix; λ_θ: Circumferential stretch, $\lambda_\theta = \frac{r}{R}$; λ_z: Longitudinal stretch, $\lambda_z = \frac{l}{L}$; MAP: Mean arterial pressure,

MAP = DBP + PP/3; $nS_{\theta\theta}$: Normalized circumferential direct stiffness. Normalized element of the stiffness matrix from the linearization of the nonlinear model. $nS_{\theta\theta} = \frac{S_{\theta\theta}}{S_{\theta\theta}}$; $nS_{\theta z}$: Normalized circumferential cross-coupled stiffness. Normalized element of the stiffness matrix from the linearization of the nonlinear model. $nS_{\theta\theta} = \frac{S_{\theta z}}{S_{\theta\theta}}$; $nS_{z\theta}$: Normalized longitudinal cross-coupled stiffness. Normalized element of the stiffness matrix from the linearization of the nonlinear model. $nS_{\theta\theta} = \frac{S_{z\theta}}{S_{\theta\theta}}$; nS_{zz}: Normalized longitudinal direct stiffness. Normalized element of the stiffness matrix from the linearization of the nonlinear model, $nS_{\theta\theta} = \frac{S_{zz}}{S_{\theta\theta}}$; PIMMP: Parameter identification method for mechanical parameters; $R_{\theta\theta}$: Ratio of stress from a small change in baseline stretch and baseline stiffness for circumferential direct stiffness. How circumferential (θ) stretch affects circumferential (θ) stress. $R_{\theta\theta} = \frac{\sigma_\theta^{L,\theta p} - \sigma_\theta^L}{\sigma_\theta^L}$; $R_{\theta z}$: Ratio of stress from a small change in baseline stretch and baseline stiffness for circumferential cross-coupled stiffness. How longitudinal (z) stretch affects circumferential (θ) stress. $R_{\theta z} = \frac{\sigma_\theta^{L,zp} - \sigma_\theta^L}{\sigma_\theta^L}$; $R_{z\theta}$: Ratio of stress from a small change in baseline stretch and baseline stiffness for longitudinal cross-coupled stiffness. How circumferential (θ) stretch affects longitudinal (z) stress. $R_{z\theta} = \frac{\sigma_z^{L,\theta p} - \sigma_z^L}{\sigma_z^L}$; R_{zz}: Ratio of stress from a small change in baseline stretch and baseline stiffness for longitudinal direct stiffness. How longitudinal (z) stretch affects longitudinal (z) stress. $R_{zz} = \frac{\sigma_z^{L,zp} - \sigma_z^L}{\sigma_z^L}$; Pa: Pascal. Unit for pressure; PP: Pulse pressure, SBP − DBP; PWV: Pulse wave velocity; SBP: Systolic blood pressure; SD: Standard deviation; VSMC: Vascular smooth muscle cells; σ_θ: Circumferential wall stress (symbol commonly used in mechanical engineering); σ_z: Longitudinal wall stress (symbol commonly used in mechanical engineering); σ_r: Radial wall stress (symbol commonly used in mechanical engineering); τ_w: Wall shear stress (symbol commonly used in mechanical engineering).

Author Contributions
JK, JS and TL contributed to the study design. Material preparation and data acquisition were performed by TL. Model computation and statistical analysis were performed by JK. Interpretation of data was made by JK, JS, TL and JE. The first draft of the manuscript was written by JK. Iterative versions of the manuscript were critically revised and commented on by JS, CJC, TL and JE. All authors read and approved the final manuscript.

Funding
Open access funding provided by Linköping University. This study was funded by grants from *Region Östergötland*, Medical Faculty Linköping University, the Swedish Research Council Grant 12661 and the Swedish Heart–Lung Foundation. The above funding sources supported the salary of JK but did not have any role in the design of the study and collection, analysis and interpretation of data or in writing the manuscript.

Availability of Data and Material
The datasets used and/or analyzed during the current study are available from the corresponding author on reasonable request.

Declarations

Conflict of interest
The authors declare that they have no competing interest.

Ethics approval
The study was approved by the Ethics Committee, Lund University, Sweden (Dnr LU457-90, Forskningsetiska kommittén Lund, 1991-04-17).

Consent to participate
Each subject gave written informed consent, according to the Helsinki declaration.

Consent for publication
The authors give their consent for publication of this manuscript.

Author details
[1]Department of Clinical Physiology in Linköping, Linköping University, 581 83 Linköping, Sweden. [2]Department of Medical and Health Sciences, Linköping University, 581 83 Linköping, Sweden. [3]Solid Mechanics, Department of Management and Engineering, Linköping University, 581 83 Linköping, Sweden. [4]Department of Thoracic and Vascular Surgery in Linköping, Linköping University, 581 83 Linköping, Sweden. [5]Center for Medical Image Science and Visualization, Linköping University, 581 83 Linköping, Sweden.

Received: 10 July 2022 Accepted: 9 September 2022
Published online: 25 November 2022

References

1. Laurent S, Cockcroft J, Van Bortel L, Boutouyrie P, Giannattasio C, Hayoz D, Pannier B, Vlachopoulos C, Wilkinson I, Struijker-Boudier H. Expert consensus document on arterial stiffness: methodological issues and clinical applications. Eur Heart J. 2006;27(21):2588–605.
2. Lacolley P, Regnault V, Segers P, Laurent S. Vascular smooth muscle cells and arterial stiffening: relevance in development, aging, and disease. Physiol Rev. 2017;97(4):1555–617.
3. Humphrey JD, Dufresne ER, Schwartz MA. Mechanotransduction and extracellular matrix homeostasis. Nat Rev Mol Cell Biol. 2014;15(12):802–12.
4. Humphrey JD, Eberth JF, Dye WW, Gleason RL. Fundamental role of axial stress in compensatory adaptations by arteries. J Biomech. 2009;42(1):1–8.
5. Wagenseil JE, Mecham RP. Vascular extracellular matrix and arterial mechanics. Physiol Rev. 2009;89(3):957–89.
6. Reesink KD, Spronck B. Constitutive interpretation of arterial stiffness in clinical studies: a methodological review. Am J Physiol Heart Circul Physiol. 2019;316(3):H693–709.
7. Schulze-Bauer CA, Holzapfel GA. Determination of constitutive equations for human arteries from clinical data. J Biomech. 2003;36(2):165–9.
8. Stalhand J. Determination of human arterial wall parameters from clinical data. Biomech Model Mechanobiol. 2009;8(2):141–8.
9. Gade JL, Stalhand J, Thore CJ. An in vivo parameter identification method for arteries: numerical validation for the human abdominal aorta. Comput Methods Biomech Biomed Eng. 2019;22:1–16.
10. Astrand H, Stalhand J, Karlsson J, Karlsson M, Sonesson B, Lanne T. In vivo estimation of the contribution of elastin and collagen to the mechanical properties in the human abdominal aorta: effect of age and sex. J Appl Physiol (1985). 2011;110(1):176–87.
11. Astrand H, Ryden-Ahlgren A, Sandgren T, Lanne T. Age-related increase in wall stress of the human abdominal aorta: an in vivo study. J Vasc Surg. 2005;42(5):926–31.
12. Holzapfel GA, Gasser TC, Ogden RW. A new constitutive framework for arterial wall mechanics and a comparative study of material models. J Elast. 2000;61(1):1–48.
13. Fung YC. Biomechanics: circulation. 2nd ed. New York: Springer; 1997.
14. Horny L, Adamek T, Zitny R. Age-related changes in longitudinal prestress in human abdominal aorta. Arch Appl Mech. 2012;83(6):875–88.
15. Stalhand J, Klarbring A, Karlsson M. Towards in vivo aorta material identification and stress estimation. Biomech Model Mechanobiol. 2004;2(3):169–86.
16. Fung YC. Elasticity of soft tissues in simple elongation. Am J Physiol Heart Circul Physiol. 1967;213(6):1532–44.
17. Humphrey JD: *Cardiovascular Solid Mechanics: Cells, Tissues, and Organs*. 2002.
18. Wikström F, Råde L, Westergren B. Mathematics handbook. 6th ed. Lund: Studentlitteratur; 2019.
19. Field A. Discovering statistics using IBM SPSS statistics. 4th ed. London: Sage; 2013.

20. Pries AR, Reglin B, Secomb TW. Remodeling of blood vessels: responses of diameter and wall thickness to hemodynamic and metabolic stimuli. Hypertension. 2005;46(4):725–31.
21. Jackson ZS, Gotlieb AI, Langille BL. Wall tissue remodeling regulates longitudinal tension in arteries. Circ Res. 2002;90(8):918–25.
22. Humphrey JD. Vascular adaptation and mechanical homeostasis at tissue, cellular, and sub-cellular levels. Cell Biochem Biophys. 2008;50(2):53–78.
23. Jackson ZS, Dajnowiec D, Gotlieb AI, Langille BL. Partial off-loading of longitudinal tension induces arterial tortuosity. Arterioscler Thromb Vasc Biol. 2005;25(5):957–62.
24. Nichols WW, McDonald DA, O'Rourke MF. Properties of the arterial wall: practice. In: McDonald's Blood flow in arteries : theoretical, experimental and clinical principles. 4th ed. London: Hodder Arnold; 2005. p. 67–93.
25. Erbel R, Alfonso F, Boileau C, Dirsch O, Eber B, Haverich A, Rakowski H, Struyven J, Radegran K, Sechtem U, et al. Diagnosis and management of aortic dissection: Task Force on Aortic Dissection, European Society of Cardiology. Eur Heart J. 2001;22(18):1642–81.
26. Sonesson B, Hansen F, Stale H, Länne T. Compliance and diameter in the human abdominal aorta—the influence of age and sex. Eur J Vasc Surg. 1993;7(6):690–7.
27. Natoli AK, Medley TL, Ahimastos AA, Drew BG, Thearle DJ, Dilley RJ, Kingwell BA. Sex steroids modulate human aortic smooth muscle cell matrix protein deposition and matrix metalloproteinase expression. Hypertension. 2005;46(5):1129–34.
28. Rajkumar C, Kingwell BA, Cameron JD, Waddell T, Mehra R, Christophidis N, Komesaroff PA, McGrath B, Jennings GL, Sudhir K, Dart AM. Hormonal therapy increases arterial compliance in postmenopausal women. J Am Coll Cardiol. 1997;30(2):350–6.
29. Dingemans KP, Teeling P, Lagendijk JH, Becker AE. Extracellular matrix of the human aortic media: an ultrastructural histochemical and immunohistochemical study of the adult aortic media. Anat Rec. 2000;258(1):1–14.
30. Lehoux S, Castier Y, Tedgui A. Molecular mechanisms of the vascular responses to haemodynamic forces. J Intern Med. 2006;259(4):381–92.
31. Clark JM, Glagov S. Transmural organization of the arterial media. The lamellar unit revisited. Arteriosclerosis. 1985;5(1):19–34.
32. Raspanti M, Protasoni M, Manelli A, Guizzardi S, Mantovani V, Sala A. The extracellular matrix of the human aortic wall: ultrastructural observations by FEG-SEM and by tapping-mode AFM. Micron. 2006;37(1):81–6.
33. Qiu H, Depre C, Ghosh K, Resuello RG, Natividad FF, Rossi F, Peppas A, Shen Y-T, Vatner DE, Vatner SF. Mechanism of gender-specific differences in aortic stiffness with aging in nonhuman primates. Circulation. 2007;116(6):669–76.
34. Holzapfel GA, Sommer G, Gasser CT, Regitnig P. Determination of layer-specific mechanical properties of human coronary arteries with nonatherosclerotic intimal thickening and related constitutive modeling. Am J Physiol Heart Circul Physiol. 2005;289(5):H2048–58.
35. Singh SI, Devi LS. A study on large radial motion of arteries in vivo. J Biomech. 1990;23(11):1087–91.